

Unquenched QCD simulation results

Sinya Aoki^{a*}

^aInstitute of Physics, University of Tsukuba,
Tsukuba, Ibaraki 305-8571, JAPAN

The recent progress on unquenched QCD simulations is critically reviewed. After some discussions on problems and subtleties in unquenched simulations, hadron spectra obtained from both quenched and unquenched simulations are compared among various gauge and quark actions. It is found that the Edinburgh plot does not agree in the continuum limit between Wilson and KS quark actions even in quenched QCD. Dynamical quark effects on hadron spectra, in particular, on meson masses are then presented for Wilson-type quark actions. Finally dynamical quark effects on other quantities such as the topological susceptibility and the flavor-singlet meson mass are discussed.

1. Introduction

An ultimate goal of lattice QCD simulations is to numerically solve the dynamics of the strong interaction. Due to lack of enough computational resources, however, a large part of simulations so far have been performed within the quenched approximation. Recent results from high statistical simulations[1] identified errors associated with the quenched approximation: predicted hadron masses in the continuum limit, in particular those containing strange quarks, differ from corresponding experimental values as large as 10%. The effect of the quark determinant must remove these differences.

In this talk I review recent progress in unquenched QCD simulations. I will survey the quality of current unquenched simulations and to what extent dynamical quark effects can be seen, in the light of the precise results from the quenched simulation[1].

I first discuss several problems in unquenched simulations such as the auto-correlation and the finite size effect, which slowed down a lot unquenched simulations in the past. Although these problems still exist, they are not a main obstruction anymore. A brief consideration on the scale determination and a theoretical discussion on the problem of changing the quark mass in

unquenched QCD then follow.

Using a large part of this report hadron spectra are analyzed for KS and Wilson quark actions in parallel, to compare the quality of data. Unfortunately and unexpectedly I notice that they disagree in the continuum limit even for the quenched case, as we will see.

In the main part the effect of dynamical quarks on hadron spectra is discussed in the case of the Wilson quark action. After the chiral extrapolation in the sea quark mass, the effect becomes most visible, in particular on the hyper-fine splitting of mesons, which consequently removes a large part of the quenching error in strange meson spectra.

In the last part, the string breaking, the topological susceptibility and the flavor-singlet meson mass are discussed in connection with the dynamical quark effect. This year mostly positive results are reported on all these quantities.

Some important subjects such as quark masses, weak-matrix elements and heavy quark physics in unquenched QCD will not be covered. Please see other reviews on these topics[2–4].

2. Recent unquenched QCD simulations

Recent large-scale unquenched simulations are summarized in Table 1, where N_f is the number of flavors of dynamical quarks. Throughout

*saoki@het.ph.tsukuba.ac.jp

Table 1
Summary of recent unquenched QCD simulations

action	a (fm)	La (fm)	m_{PS}/m_V
$N_f = 2$			
PW[10]	0.086	1.4	0.69–0.83
PW[11]	0.086	2.0	0.55, 0.7
PKS[12]	0.09	1.5	0.57–0.70
PKS[13]	0.10–0.32	2.4–3.8	0.3–0.8
PC(1.76)[14]	0.12	1.0–1.9	0.67–0.86
RC(TP)[15]	0.11–0.22	2.5–2.6	0.55–0.81
PC(NP)[16]	0.10	1.6	0.58–0.83
PC(NP)[17]	0.10	1.2–2.0	0.60–0.80
$N_f = 3$			
SKS(I)[18]	0.14	2.8	0.50–0.94

this paper, the following abbreviations are used to distinguish different lattice actions in simulations. The first letter stands for the gauge action: P = Plaquette, R = RG improved[5], S = Symanzik improved[6], while the second or more letters represent the quark action: W = Wilson, KS = Kogut-Susskind, KS(I) = Improved KS[7,8] C(X) = Clover[9] with $C_{SW} = X$, where TP = Tadpole estimated value and NP = Non-Perturbative value. For example, PW stands for the plaquette gauge action and the Wilson quark action while RC(TP) for the RG improved gauge action and the clover quark action with the tadpole estimated value for C_{SW} .

Simulations have been carried out at several lattice spacings for the PKS[13] and the RC(TP)[15] actions. Using data from these simulations one can make extrapolations to the continuum limit.

3. Several remarks on unquenched simulations

In this section several remarks are given on problems associated with unquenched simulations.

3.1. Auto-correlations

Since unquenched simulations are very time-consuming, it is better to perform hadron measurements as often as possible. In such cases, one has to multiply statistical errors by $\sqrt{2\tau_{int}}$, where τ_{int} is the integrated auto-correlation time of the simulation, or equivalently, one should increase

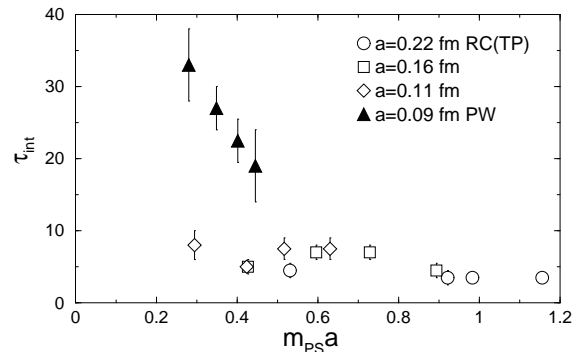


Figure 1. Integrated auto-correlation time for the number of iterations, $\tau_{int}^{N_{inv}}$ in the HMC algorithm, as a function of PS meson mass, for the PW action[10,11,19] and the RC(TP) action[15].

the bin-size of the Jack-knife analysis until the error reaches a plateau.

The integrated auto-correlation time for an observable \mathcal{O} is defined as

$$\tau_{int}^{\mathcal{O}} = \lim_{t \rightarrow \infty} \left[\frac{1}{2} + \sum_{t'=1}^t \frac{C^{\mathcal{O}}(t')}{C^{\mathcal{O}}(0)} \right] \quad (1)$$

where $C^{\mathcal{O}}(t)$ is the auto-correlation function for \mathcal{O} given by

$$C^{\mathcal{O}}(t) = \langle \mathcal{O}(s)\mathcal{O}(s+t) \rangle_s - \langle \mathcal{O}(s) \rangle_s \cdot \langle \mathcal{O}(s+t) \rangle_s \quad (2)$$

$$\text{with } \langle F(s) \rangle_s \equiv \frac{1}{n} \sum_{s=1}^n F(s).$$

The auto-correlation time depends on the observable and, of course, the simulation algorithm. In unquenched QCD, π meson propagator at a given time, or the number of iterations for inversions of $D^\dagger D$ where D is a lattice Dirac operator, seems to have a long auto-correlation time. In Fig. 1, τ_{int} for the number of iterations N_{inv} in the HMC algorithm is plotted as a function of the PS meson mass, which corresponds to $m_{PS}/m_V \geq 0.55$, in the case of Wilson-type (Wilson/Clover) quark actions [10,11,15,19]. We estimate $\tau_{int}^{N_{inv}} \simeq 5 \sim 40$, and similarly obtain $\tau_{int}^{\pi} \simeq 5 \sim 40$. One should keep in mind that an accurate estimate of error for auto-correlation time requires $O(100 - 1000) \times \tau_{int}$ data, so errors in these figures may well be under-estimated. These τ_{int} are less or comparable to $\tau_{int}^{\pi} \simeq 40$ for

the KS quark action[13]. It is noted that $\tau_{int}^{\pi, N_{inv}}$ for the PW are larger than those for the RC action. This may be caused by the difference of gauge actions, lattice spacings or simulation parameters in the HMC algorithm.

From a practical point of view, $\tau_{int} \simeq 10$ is short enough, even $\tau_{int} \simeq 40$ is not so bad, since recent unquenched simulations can accumulate 8000 trajectories or more, which correspond to roughly 100–400 independent configurations.

It is expected that $\tau_{int}^{N_{inv}}$ increases as the quark mass (PS meson mass) decreases, according to the scaling formula

$$\tau_{int}^{N_{inv}} = A \cdot (m_{PS}a)^{-Z}. \quad (3)$$

From data at $a \simeq 0.09$ fm for the PW action in the figure, one obtains $Z = 1.20(5)$ [19], which predicts a moderate number, $\tau_{int}^{N_{inv}} \simeq 200$, for $m_{PS} = 140$ MeV. Since this number is expected to be smaller for the RC action, the auto-correlation may not be a major obstruction toward lighter quark masses in unquenched simulations.

It has been observed that the topological charge Q has a long auto-correlation time of the order of a few hundred trajectories or more in unquenched HMC simulations with the KS quark action. This makes a measurement of the topological susceptibility very difficult. On the other hand, recent unquenched simulations give $\tau_{int}^Q \simeq 30 - 40$ for the RC(TP) action, at $a = 0.11$ fm and $m_{PS}/m_V = 0.55 - 0.81$ [15]. This value of τ_{int}^Q is small enough to make the calculation of the topological susceptibility possible. This difference may be explained by the fact that the KS fermion determinant suppresses the change of the topological charge at small quark masses due to chiral symmetry. Further investigations, however, will be needed to confirm this speculation, for example, by employing the domain-wall quark action in unquenched simulations.

In conclusion the auto-correlation is not a major problem for present unquenched simulations, except for the case of the topological charge with the KS quark action[21].

3.2. Finite size effects

While finite size effects on hadron masses are known to be much stronger in unquenched QCD

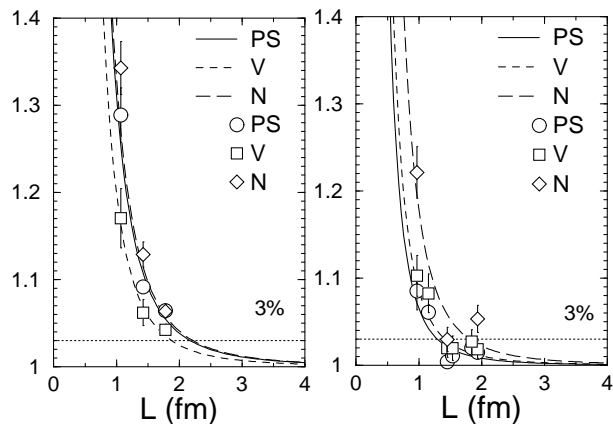


Figure 2. Finite size errors on hadron masses $(m_H(L) - m_H)/m_H$ for $H = \text{PS}, \text{V}, \text{N}$ as a function of spatial extension L (fm), in the case of KS (left)[22,23] and clover(right)[14,17] quark actions.

than in quenched QCD for the KS quark action[22,23], recent unquenched simulations[14,17] suggest that finite size effects for Wilson-type quark actions are milder.

To compare results from the two types of actions directly, hadron masses at a finite extension L are fitted by the form

$$m_H(L) = m_H + \frac{c}{L^3}, \quad (4)$$

which is found to be good for the range of L in the current simulations[22], and therefore is used as a working hypothesis for the comparison. Relative errors, $(m_H(L) - m_H)/m_H$, for $H = \text{PS}$ (Pseudo Scalar), V (Vector) and N (Nucleon), are plotted as a function of L in Fig. 2, at $a \simeq 0.09$ fm and $m_{PS}/m_V \simeq 0.68$ for the KS quark action[22,23] and at $a \simeq 0.12$ fm and $m_{PS}/m_V \simeq 0.72$ for the clover quark action[14,17]. At similar lattice spacings and m_{PS}/m_V , the size effect seems to be larger for the KS quark.

Using data currently available, the lattice size L (fm) which gives a 3% relative finite size error, $(m_H(L) - m_H)/m_H \simeq 0.03$, is summarized in Table 2.

From Fig.2 and table 2, one observes that the size effect is larger for the KS quark action than for the Wilson-type action. Moreover patterns of the size effect are different: size effects of PS

Table 2
Lattice size $L(\text{fm})$ which give 3% relative errors.

m_{PS}/m_V	$a(\text{fm})$	PS	V	N
KS				
0.5	0.2	1.2	1.9	2.2
	0.09	2.6	2.2	2.6
0.68	0.09	2.2	2.0	2.3
Wilson-type				
0.72	0.12	1.4	1.5	1.8
0.75	0.12	1.0	1.4	
0.8	0.12	1.1	1.3	1.7

and N are comparable and larger than that of V for the KS quark action while the size effect of N dominates for the Wilson-type quark action. This difference is a part of scaling violation since finite size effect is universal in the continuum limit, and it may be caused by the chiral properties of the two actions: the KS quark retains chiral symmetry while the Wilson-type quark breaks it explicitly. Another possibility is that the “effective” lattice size for the KS quark may be smaller than the lattice size for the Wilson quark, due to the spread of the KS quark over a hyper-cube in the spinor-flavor interpretation. Obvious disadvantages of Wilson-type quarks such as the absence of chiral symmetry, $O(a)$ scaling violation and larger costs of numerical simulations are partly compensated by this milder finite size effect.

3.3. Common scale

One has to fix a scale to compare results in different simulations. In quenched simulations, it may be easier and better to use a scale determined only by the gauge action such as the string tension. In unquenched simulations, however, all quantities depend on quark actions and quark masses as well as the gauge action and the gauge coupling constant.

For the common scale in unquenched simulations, one had better to use the Sommer scale r_0 [24], which is given by

$$r_0^2 \frac{dV(r)}{dr} \Big|_{r=r_0} = 1.65, \quad (5)$$

where $V(r)$ is the static quark potential.

This quantity, estimated as $r_0 \simeq 0.49 \text{ fm}$, is insensitive to either the short-distance physics of

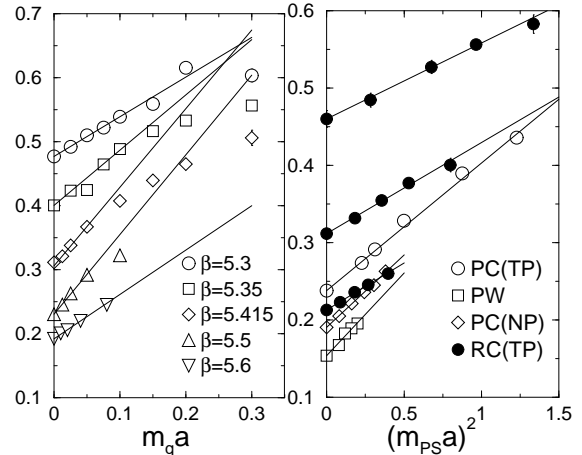


Figure 3. (Left) The quark mass dependence of the inverse of the Sommer scale for the PK action[25]. (Right) The same for PC(TP)[14], PW[26], RC(NP)[17] and RC(TP)[15] actions. Lines are fits as explained in the text.

QCD such as the Coulomb term or the long distance one represented by string breaking. In simulations r_0 is accurately determined by numerical derivative of the potential[24] or by the relation $r_0^2 = (c + 1.65)/\sigma$, where the string tension σ and the Coulomb coefficient c are extracted from the fit of $V(r)$. Two methods give consistent values of r_0 with reasonably small errors[18].

The quark mass dependence of the Sommer scale is shown in Fig.3, where the vertical axis is the inverse of the Sommer scale, while the horizontal one is the bare quark mass for the KS quark action[25] or the PS meson mass squared for Wilson-type quark actions[14,15,17,26]. One can easily obtain the value of r_0 in the chiral limit, fitting the data for small enough quark masses by the linear form

$$\frac{a}{R_0} = \frac{a}{r_0} + A \cdot M, \quad (6)$$

where $M = m_q a$ or $m_{\text{PS}}^2 a^2$.

Later the Sommer scale at $M \neq 0$ becomes necessary. For distinction I use R_0 in such cases instead of r_0 , which stands for exclusively the value in the chiral limit.

3.4. Changing quark mass

In unquenched simulations, it is non-trivial to change the quark mass while keeping the lattice spacing constant. In a standard method one varies the bare quark mass $m_q a$ at fixed β [10–15,17], determining the lattice spacing in the chiral limit or at the physical point of $m_{\text{PS}}/m_V = 0.135/0.77$. In recent simulations[16,18] one employs a new method in which both $m_q a$ and β are varied to keep R_0 constant, claiming that the lattice spacing becomes smaller at smaller quark masses otherwise. In this subsection I will discuss if this claim is true.

First of all it is noted that the lattice spacing at different quark masses can not be compared in principle since no experimental input is available away from the physical quark mass.

Let me discuss a relation between a and bare parameters in QCD using the running coupling constant $\bar{g}^2(L)$ instead of R_0 to see a difference of two methods, since the perturbative expansion in an $O(a)$ improved theory is available for $\bar{g}^2(L)$ as[27]

$$\bar{g}^2(L) = g_0^2 + g_0^4 [\beta_0 \log(L/a) + f(m_R L) + k m_R a] + O(a^2, g_0^6), \quad (7)$$

where g_0^2 is the bare coupling constant, L is the lattice size, m_R is the renormalized quark mass.

The mass-independent renormalization scheme is defined through the renormalized coupling constant \tilde{g}_R^2 , defined by

$$g_R^2 = \tilde{g}_0^2 [1 - \tilde{g}_0^2 \beta_0 \log(\mu a)] + O(\tilde{g}_0^6), \quad (8)$$

where μ is the renormalization scale. This scheme can be easily related to the \overline{MS} scheme. Clearly the standard method of unquenched simulations corresponds to this scheme, since a depends only on g_0^2 for a fixed g_R^2 . The running coupling becomes

$$\bar{g}^2(L) = \tilde{g}_R^2 + \tilde{g}_R^4 [\beta_0 \log(L\mu) + f(m_R L) + k m_R a] + O(a^2, \tilde{g}_R^6), \quad (9)$$

which has $m_R a$ scaling violation even in the $O(a)$ improved theory, in addition to the physical mass dependence $f(m_R L)$. Therefore the analogy suggests that R_0 has scaling violation of $m_R a$ as well

as the physical quark mass dependence in this scheme.

The mass-dependent scheme is specified by

$$\hat{g}_R^2 = g_0^2 [1 + g_0^2 \{-\beta_0 \log(\mu a) + f(m_R L) + k m_q a\}] + O(g_0^6), \quad (10)$$

where m_q is the bare quark mass. The lattice spacing a depends on both g_0^2 and $m_q a$ for a fixed \hat{g}_R^2 , in such a way that the running coupling becomes mass-independent:

$$\bar{g}^2(L) = \hat{g}_R^2 + \hat{g}_R^4 \beta_0 \log(L\mu) + O(a^2, \hat{g}_R^6). \quad (11)$$

Up to $O(a^2)$ ambiguity one can define the relation between g_0^2 and $m_q a$ so that $\bar{g}^2(L)$ instead of \hat{g}_R^2 becomes constant. In other words the new method of unquenched simulations corresponds to this renormalization scheme, which keeps $O(a)$ improvement in \bar{g}^2 while has a complicated relation to \overline{MS} scheme.

This consideration concludes that two methods of changing quark mass in unquenched simulations correspond to different renormalization schemes and that the lattice spacing is kept constant in both methods, contrary to the claim of ref.[16,18].

Ref. [27] has proposed another renormalization scheme, called an improved mass-independent scheme, whose renormalized coupling constant is defined by

$$\tilde{g}_R^2 = \tilde{g}_0^2 [1 - \tilde{g}_0^2 \beta_0 \log(\mu a)] + O(\tilde{g}_0^6) \quad (12)$$

where $\tilde{g}_0^2 = (1 + b_g m_q a) g_0^2$ is called an improved bare coupling constant with $b_g = k g_0^2 + O(g_0^4)$. In this scheme a depends on both g_0^2 and $m_q a$ through \tilde{g}_0^2 for a fixed \tilde{g}_R^2 , while the relation of this scheme to the \overline{MS} scheme remains simple since the mass-dependence in \tilde{g}_0^2 vanishes as $O(a)$. The running coupling constant in this scheme has a mass-dependence and is $O(a)$ improved:

$$\bar{g}^2(L) = \tilde{g}_R^2 + \tilde{g}_R^4 [\beta_0 \log(L\mu) + f(m_R L)] + \dots \quad (13)$$

Let me close this section by suggesting two options for unquenched simulations in the future. One can keep using the standard mass-independent scheme with the special care about $m_q a$ scaling violation, which may not be so large for light and strange quarks. One can instead try

the improved mass-independent scheme with either the perturbative estimate for b_g , where the 1-loop value is available[28] or the non-perturbative estimate for b_g , which seems possible by the method of ref. [29].

4. Hadron spectra: Wilson vs. KS quarks

In order to disentangle the dynamical quark effect from the scaling violation, one has to compare unquenched results with quenched ones in the continuum limit. Although precise quenched hadron spectra have already been obtained with the PW action[1], it is better to confirm the results with different actions. Such a comparison becomes more important in unquenched QCD, where it is much harder to control the continuum extrapolation. Therefore, in this section, hadron spectra in the continuum limit are systematically compared between Wilson and KS quark actions.

4.1. Edinburgh plot in quenched QCD

In the continuum limit of quenched QCD the nucleon mass is found to be a little smaller than the experimental value for the PW action[1] while it is consistent with the experimental value for the KS action[30]. To see if this small difference is caused by the ambiguity associated with the chiral extrapolation, the Edinburgh plot(m_N/m_V vs. m_{PS}/m_V) in the continuum limit of quenched QCD is shown in the upper part of Fig. 4, for PKS[30], PW[1] and RC(TP)[15] actions.

Surprisingly results between Wilson and KS quark actions in the continuum limit of quenched QCD do not agree at all in the whole range of quark masses. It should be noted, however, that the Edinburgh plot from the PW action is consistent with the one from the RC(TP) action, ensuring an agreement among Wilson-type actions in the continuum limit.

Neither the finite size effect nor the chiral extrapolation can be a main source for this discrepancy, since the volume is large enough ($La \simeq 3$ fm for PW, $2.6 \sim 3$ fm for PKS) and the discrepancy is significant in the whole range of quark masses.

To investigate the quality of the continuum extrapolation, m_N/m_V is shown in the lower part of Fig. 4 as a function of the lattice spacing $m_V a$

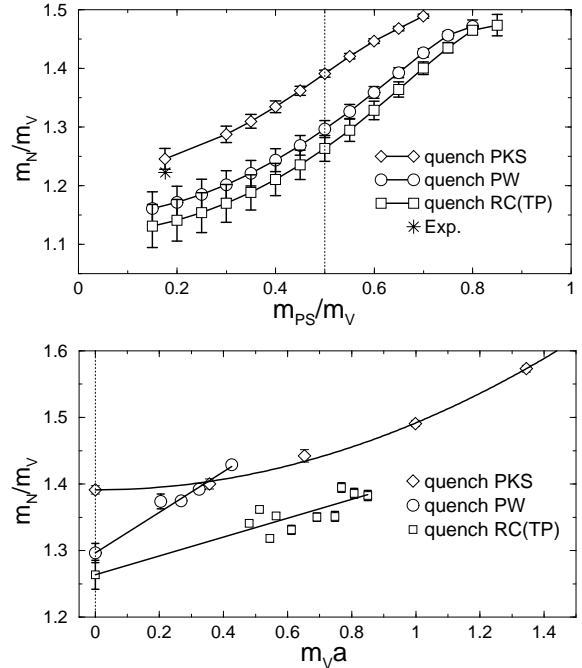


Figure 4. (Upper) The Edinburgh plot(m_N/m_V vs m_{PS}/m_V) in quenched QCD at $a = 0$ for PKS[30], PW[1] and RC(TP)[15] actions. (Lower) m_N/m_V as a function of $m_V a$ at $m_{PS}/m_V = 0.5$ for same actions.

at $m_{PS}/m_V = 0.5$, denoted by the vertical line in the Edinburgh plot, where both finite size effect and ambiguity of the chiral extrapolation should be small.

Although the quenched PW result has larger scaling violation than the quenched RC(TP) result, they agree in the continuum limit, concluding that the continuum extrapolation is controlled for Wilson-type quark actions. The scaling violation of the quenched PKS result is well fitted quadratically in $m_V a$, which is a leading behavior theoretically expected for the KS quark action[31]. It is therefore clear that the discrepancy between quenched results is not caused by the continuum extrapolations. I have to conclude that the discrepancy remains unexplained.

4.2. Edinburgh plot in unquenched QCD

The analysis in the previous subsection is applied also to unquenched results for PKS[13] and

RC(TP)[15] actions, where the finite size effect is expected to be significant, in particular for lighter quark masses. The upper part of Fig. 5 shows the Edinburgh plot in the continuum limit, which gradually flattens for the RC(TP)[15] while continuously decreases for the PKS[13] toward lighter quark masses, together with results directly obtained by simulations at non-zero a without extrapolations. The behavior for the RC(TP) indicates the existence of the finite size effect as well as the difficulty of the chiral extrapolation from the restricted range of quark masses such that $m_{\text{PS}}/m_{\text{V}} \geq 0.55$. On the other hand, the behavior for the PKS, which is irregular at non-zero, in particular larger a , makes both chiral and continuum extrapolations difficult. Consequently, the quality of data at lighter quark masses for both actions is insufficient for the reliable continuum extrapolation in the Edinburgh plot. Therefore I concentrate on results at heavy masses, where the disagreement between the two actions is already manifest.

The lower part of Fig. 5 shows $m_{\text{N}}/m_{\text{V}}$ as a function of the lattice spacing $m_{\text{V}}a$ at $m_{\text{PS}}/m_{\text{V}} = 0.5$, which is obtained by the interpolation for the PKS action or by a little extrapolation for the RC(TP) action. The scaling violation is not so significant for both RC(TP) and PKS actions. In particular the result for the latter is well fitted quadratically in $m_{\text{V}}a$. Two results largely deviate even at non-zero a , and the difference stays almost constant toward the continuum limit. Therefore the deviation is not brought into by the continuum extrapolation, though the linear continuum extrapolation for PC(TP) data might be affected a little by higher order terms such as $a \log a$ or a^2 . The lattice size, $La \simeq 2.5$ fm for the RC(TP) or 2.4 fm for the PKS, may not be large enough at $m_{\text{PS}}/m_{\text{V}} = 0.5$ in unquenched QCD. As mentioned in Sect.3.1, there may be 3% error in m_{N} for the KS quark action at $La \simeq 2.6$ fm and $a \simeq 0.1$ fm. Although no data are available for the Wilson quark action at this $m_{\text{PS}}/m_{\text{V}}$, the error is expected to be smaller than the KS quark action. With all systematics together, it may be too early to conclude that results between Wilson and KS quark actions disagree in the continuum limit at $m_{\text{PS}}/m_{\text{V}} = 0.5$. Further inves-

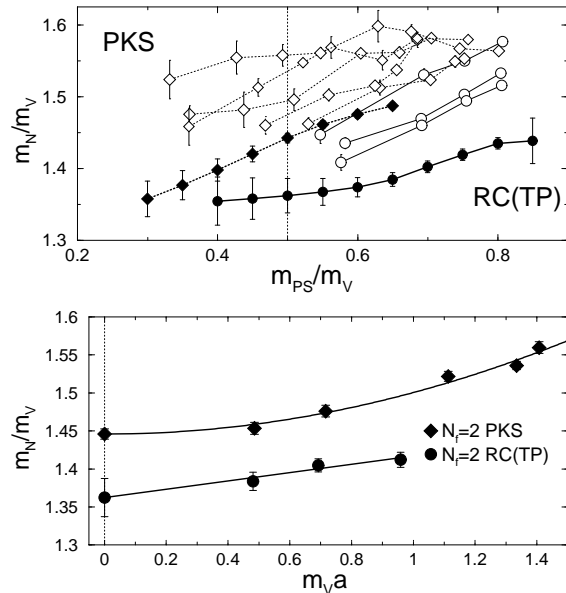


Figure 5. (Upper) The Edinburgh plot in unquenched QCD for the PKS action(diamonds)[13] and the RC(TP) action(circles)[15]. Open symbols represent data at $a = 0.32, 0.28, 0.23, 0.15, 0.10$ fm for the former and $0.22, 0.16, 0.11$ fm for the latter, from above to below, while solid symbols correspond to results in the continuum limit. (Lower) $m_{\text{N}}/m_{\text{V}}$ as a function of $m_{\text{V}}a$ at $m_{\text{PS}}/m_{\text{V}} = 0.5$ for same actions.

tigations, in particular on the finite size effect or at larger mass ratios such that $m_{\text{PS}}/m_{\text{V}} = 0.6$ to avoid the chiral extrapolation, are urgently needed to draw definite conclusions.

4.3. Hadron spectra normalized by R_0

In the previous subsection, the discrepancy in the Edinburgh plot between Wilson and KS quark actions became manifest in the continuum limit, in particular, for the quenched case. However, since the Edinburgh plot represents the relation among mass ratios, it is difficult to find a source responsible for the discrepancy. Alternatively, in this subsection, hadron masses normalized by the Sommer scale are considered as a function of $(m_{\text{PS}}R_0)^2$, which plays the role of quark mass. With this normalization one can keep the simple relation between m_{H} and m_{PS}^2 as long as the quark mass dependence of R_0 is sub-leading,

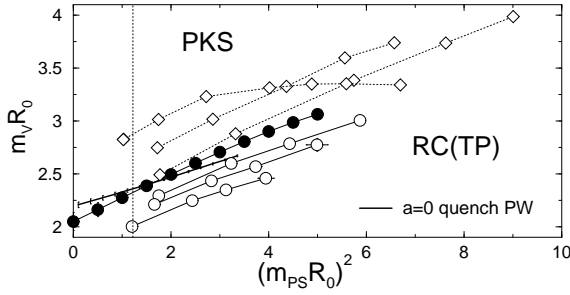


Figure 6. $m_V R_0$ as a function of $(m_{PS} R_0)^2$ in unquenched QCD for the PKS action (diamonds)[13] and the RC(TP) action (circles)[15]. Open symbols represent data at non-zero a , while solid ones in the continuum limit. Solid line represents quenched data in the continuum limit for the PW action[1] for comparison.

while still avoiding the chiral extrapolation.

In Fig. 6 $m_V R_0$ from unquenched simulations is plotted as a function of $(m_{PS} R_0)^2$ at non-zero a , for both RC(TP)[15] and PKS[13] actions, together with lines in the continuum limit from quenched PW[1] and unquenched RC(TP). Unfortunately lines in the continuum limit are not available for the PKS action.

Data at non-zero a approach the continuum limit from below ($a = 0.22, 0.16, 0.11$ fm) for RC(TP) and from above ($a = 0.21, 0.15, 0.11$ fm) for PKS. The behavior looks reasonable except for PKS at $a \simeq 0.21$ fm. Roughly speaking slopes are similar among unquenched results and steeper than the quenched one.

As before the scaling behavior is examined at $(m_{PS} R_0)^2 = 1.22$, where PKS data are available. In the left part of Fig. 7 $m_V R_0$ at $(m_{PS} R_0)^2 = 1.22$ is shown as a function of a/R_0 . The quenched PKS data[30] and SKS(I) data[32,33] agree with each other in the quadratic continuum extrapolation, and an extremely good scaling behavior is observed for the latter. The continuum values also agree with that for the PW action. Therefore no discrepancy is found for quenched vector meson masses between KS and Wilson quarks.

Similarly the scaling behavior of $m_N R_0$ is shown in the right part of Fig. 7 at $(m_{PS} R_0)^2 = 1.22$. The linear continuum extrapolation of quenched PW data[1] gives a smaller

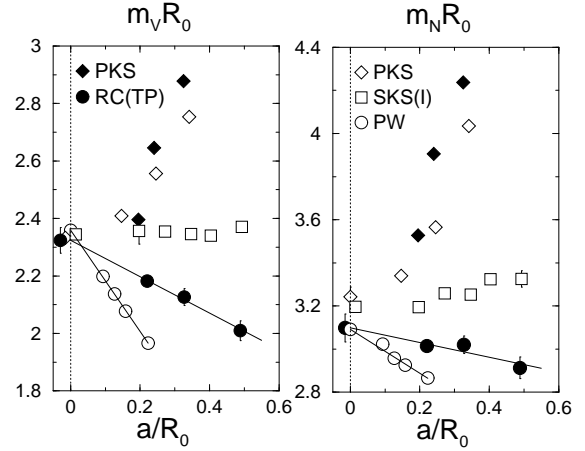


Figure 7. $m_V R_0$ (left) and $m_N R_0$ (right) as a function of a/R_0 at $(m_{PS} R_0)^2 = 1.22$, in quenched QCD (open symbols) with PW[1], PKS[30] and SKS(I)[32,33] actions and in unquenched QCD (solid symbols) with RC(TP)[15] and PKS[13] actions.

value than the quadratic one of quenched PKS data[30], which well agrees with the one of SKS(I) data[32,33].

The individual analysis for m_V and m_N suggests that a discrepancy in m_N is a main source for the disagreement in the Edinburgh plot between PW and PKS actions in quenched QCD.

For unquenched QCD, continuum extrapolations of m_V and m_N are reasonably good for the RC(TP) action[15] and agree with those for quenched QCD with PW[1], while very large scaling violations for m_V and m_N , which do not show expected a^2 behaviors, make continuum extrapolations of individual masses impossible for the PKS action[13]. However these large scaling violations in m_V and m_N cancel each other in the ratio m_N/m_V as seen in the lower part of Fig. 5.

4.4. Suggestions on further investigations

From available data so far we can not identify a definite reason for the discrepancy in the Edinburgh plot between Wilson and KS quark actions, in particular for quenched QCD, where the disagreement is found only in m_N . To completely resolve the problem, we should accumulate as many data as available for all varieties of

actions and simulations.

We should analyze the Edinburgh plot and the plot of $m_H R_0$ vs $(m_{PS} R_0)^2$, as well as their scaling behavior at $m_{PS}/m_V=0.5, 0.7$ for the former and at $(m_{PS} R_0)^2 = 1.22, 3.0$ for the latter as typical values already used in several literatures.

Even quenched results from the third type of quark actions such as domain-wall or overlap will become useful to resolve the problem.

5. Dynamical quark effects on hadron spectra

In this section, dynamical quark effects on hadron spectra are investigated, comparing data from unquenched simulations with those from quenched ones. Due to the discrepancy between Wilson and KS quark actions in the previous section, results only for Wilson-type quark actions are considered here, since more data are available so far.

5.1. Quark mass dependence in partially quenched analysis

In unquenched simulations, valence quark masses can be different from the mass of dynamical quarks (sea quark mass). In such a partially quenched analysis, the PS meson mass squared are employed for Wilson-type quark actions to specify how large the quark mass is, without chiral extrapolation necessary to define the quark mass through the critical hopping parameter.

The following equality is then assumed for the PS meson mass.

$$\begin{aligned} m_{PS, \text{val}}^2 &\equiv \frac{1}{2} [m_{PS}^2(s; v_1, v_1) + m_{PS}^2(s; v_2, v_2)] \\ &= m_{PS}^2(s; v_1, v_2) \end{aligned} \quad (14)$$

where s specifies a sea quark mass for degenerate $N_f = 2$ dynamical quarks and v_1 and v_2 denote valence quark masses in the meson. This assumption is correct at the lowest order of chiral perturbation theory and is well-satisfied numerically in data of ref. [17].

In Fig.8 $m_V(s; v_1, v_2)$ is plotted in lattice units as a function of $m_{PS, \text{val}}^2$ [17]. At a fixed sea quark mass ($K_{sea} = 0.1355$, for example, which corresponds to $m_{PS}/m_V \simeq 0.6$), data lie on one curve

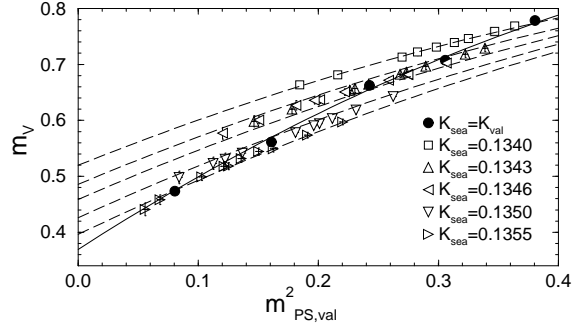


Figure 8. $m_V(s; v_1, v_2)$ in lattice units as a function of $m_{PS, \text{val}}^2$ at $\beta = 5.2$ for the PC(NP) action on a $16^3 \times 48$ lattice [17].

with some curvature, suggesting that higher order terms in $m_{PS, \text{val}}^2$ are necessary while the effect of $(m_{PS}^2(s; v_1, v_1) - m_{PS}^2(s; v_2, v_2))^2$ term is negligible. Therefore, as shown in the figure, data can be reasonably fitted by the form

$$\begin{aligned} m_V(s; v_1, v_2) &= A + B_s \cdot m_{PS, s}^2 + C_s \cdot (m_{PS, s}^2)^2 \\ &\quad + (B_v + C_{sv} \cdot m_{PS, s}^2) \cdot m_{PS, \text{val}}^2 \\ &\quad + C_v \cdot (m_{PS, \text{val}}^2)^2 \end{aligned} \quad (15)$$

with $m_{PS, s}^2 = m_{PS}^2(s; s, s)$, where all possible terms of $O(m_{PS}^4)$ are included. The fact that the intercept and the curvature of each curve depend on the sea quark mass might be interpreted as a dynamical quark effect.

To see if this is really a dynamical quark effect, the same data normalized by R_0 are shown in the left part of Fig. 9, together with quenched data at $\beta = 6.0$ and 6.2 for the same action [34]. Note that the scaling violation is negligible in the quenched case.

A curvature can not be clearly seen anymore, and a linear decrease seems steeper than the quenched one. Partly due to larger errors caused by that of R_0 , however, the fit by the form

$$\begin{aligned} R_0 \cdot m_V(s; v_1, v_2) &= A + B_s \cdot R_0^2 \cdot m_{PS}^2 \\ &\quad + B_v \cdot R_0^2 \cdot m_{PS, \text{val}}^2 \end{aligned} \quad (16)$$

can not resolve a sea quark mass dependence in the data, giving $B_s \simeq 0$. The fit with $B_s = 0$, plotted in the figure, gives a reasonable value of χ^2 , showing a steeper slope B_v ,

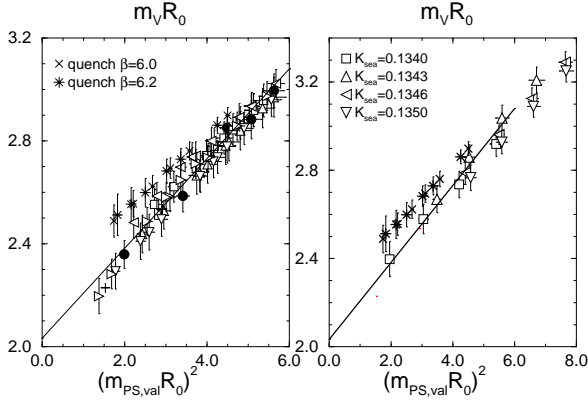


Figure 9. (Left) $R_0 m_V(s; v_1, v_2)$ as a function of $(m_{\text{PS,val}} R_0)^2$ for the PC(NP) action from the JLQCD collaboration[17], together with the quenched data for the PC(NP) action[34]. Symbols are the same in Fig. 6. (Right) The same plot for the PC(NP) action from the UKQCD collaboration[16], together with the fit line of the left figure.

which may be regarded as the dynamical quark effect. Further precise calculations will be required, however, to resolve the sea quark mass dependence of the slope B_s in this range of sea quark masses ($m_{\text{PS}}/m_V \simeq 0.6 - 0.8$), so that the dynamical quark effect is undoubtedly identified.

As mentioned before, the UKQCD collaboration has performed an unquenched simulation varying both β and $m_q a$ of PC(NP) action in order to keep R_0 constant[16]. As shown in the right part of Fig. 9, the result is consistent with the one from the fixed β simulation of the JLQCD collaboration[17], once both data are normalized by R_0 .

5.2. Chiral extrapolation

The dynamical quark effect is expected to be enhanced toward smaller sea quark masses reached by the chiral extrapolation, which is briefly described in this subsection.

The light quark mass is determined by the experimental value of m_π/m_ρ . In the present method, the ratio determines the corresponding PS meson mass, $m_{\text{PS},s} a$ by solving the equation

$$\frac{m_\pi}{m_\rho} = \frac{m_{\text{PS},s} a}{A + (B_s + B_v) m_{\text{PS},s}^2 a^2 + \dots} \quad (17)$$

where the denominator is obtained by setting $m_{\text{PS,val}}^2 = m_{\text{PS},s}^2$ in eq. (15), and the lattice spacing a is explicitly written. Hereafter $m_{\text{PS},s}^2 a^2$ is fixed to the solution of this equation, $m_{\text{PS},s} a = m_\pi a$.

There are several ways to determine the strange quark mass. The K -input uses the experimental value of m_K/m_π to determine other strange mesons, while the ϕ -input uses the experimental value of m_ϕ/m_ρ .

To compare results at different a , hadron masses are normalized by r_0 , the value of R_0 in the chiral limit.

5.3. Meson spectra at dynamical light quark masses

The vector meson mass normalized by r_0 , $m_V r_0$ in unquenched QCD is shown in the left part of Fig.10, as a function of $m_{\text{PS,val}}^2 r_0^2$, at $a = 0.11 \sim 0.22$ fm for the RC(TP) action[15] and at $a = 0.1$ for the PC(NP) action[17], together with the quenched result in the continuum limit[1]. The lines in the figure are determined by eq. (15) with $m_{\text{PS},s}^2 = m_\pi^2$ fixed, and the points on the line marked by (π, ρ) , (K, K^*) and (η_s, ϕ) are given by $m_{\text{PS}}/m_V = 0.1350/0.7684$, $0.4977/0.8961$ and $0.695/1.0194$, respectively, where $m_{\eta_s} = 0.695$ GeV is used for an unphysical η_s . The error of the line, not shown in the figure for the RC(TP) action, is roughly equal to the error of the points, where the error of r_0 is not included. The error band for the PC(NP) action includes this source of error.

The slope of unquenched data increases as a decreases, so that the slope at $a = 0.11$ fm of RC(TP) action is clearly steeper than the slope of the quenched result in the continuum limit, and closer to experiment. This is the manifestation of dynamical quark effect on hadron spectra we are looking for. The chiral extrapolation in the sea quark mass, as well as control of scaling violation, is necessary to see the effect clearly. The line for the PC(NP) at $a = 0.1$ fm, which lies a little above, seems consistent with the RC(TP) if errors from the remaining scaling violation and r_0 are taken into account.

The result of m_V can be converted into the hyper-fine splitting of mesons, and is shown in

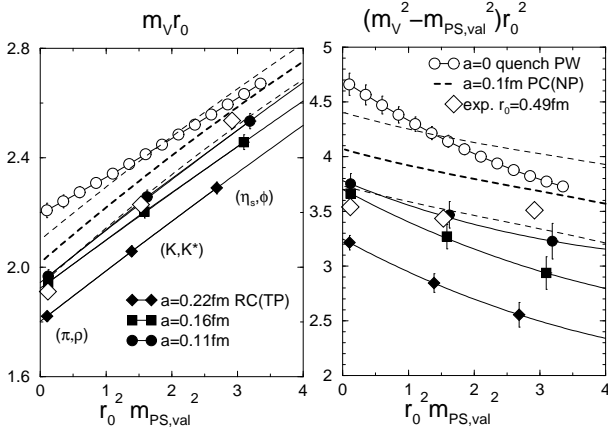


Figure 10. (Left) $m_V r_0$ (left) and (Right) $(m_V^2 - m_{PS,val}^2) r_0^2$ as a function of $m_{PS,val}^2 r_0^2$ with $m_{PS,s}^2 = m_\pi^2$ fixed, in unquenched QCD for RC(TP)[15] and PC(NP)[17] actions, together with the quenched result of the PW action[1].

the right part of Fig. 10, where $(m_V^2 - m_{PS,val}^2) r_0^2$ is plotted as a function of $m_{PS,val}^2 r_0^2$ with $m_{PS,s}^2 = m_\pi^2$ fixed. The slope of unquenched data decreases with a , and is very different from the quenched one in the continuum limit. The dynamical quark effect is most noticeable for the hyper-fine splitting normalized by r_0 .

Let me remark that a steeper slope of the hyper-fine splitting in quenched QCD means a smaller hyper-fine splitting of strange mesons than the experimental value, if the splitting between m_ρ and m_π is fixed to the experimental value.

5.4. Continuum limit of strange meson masses

In Fig. 11, the scaling behavior of ϕ and K^* meson masses from K -input, converted into GeV unit using ρ meson mass, are plotted in $N_f = 2$ unquenched QCD for RC(TP)[15] and PC(NP)[17] actions, together with the quenched result for PW[1] and RC(TP)[15] actions. Lines represent linear continuum extrapolations for the $N_f = 2$ RC(TP), quenched PW and RC(TP) results.

A large discrepancy between the experimental value and the quenched result in the continuum limit is much reduced in $N_f=2$ unquenched QCD.

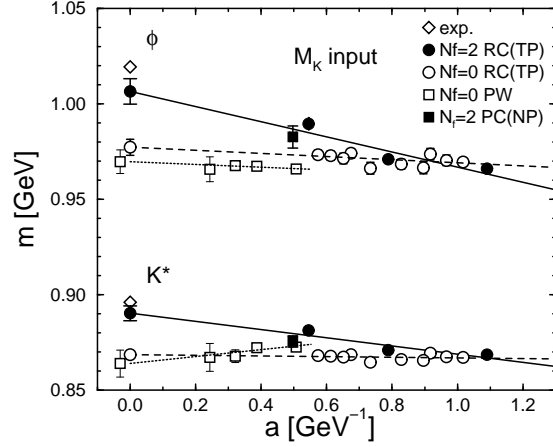


Figure 11. m_ϕ and m_{K^*} (GeV) as a function of a (GeV) in $N_f = 2$ QCD for RC(TP)[15] and PC(NP)[17] actions and in quenched QCD for PW[1] and RC(TP)[15] actions. The scale is set by m_ρ .

It will be interesting to see if the inclusion of the dynamical strange quark removes the remaining small difference.

5.5. Remark on the continuum extrapolation

Here a remark is given on the scaling behavior of perturbatively improved theories such as RC(TP), extensively employed in unquenched QCD simulations. Suppose that a renormalized observable $X(a)$ at non-zero lattice spacing a is expanded in the bare coupling constant g_0^2 as

$$X(a) = X_0 + g_0^2 [x_1^0 + a(x_1^1 + y_1^1 \log a)] + g_0^4 [x_2^0 + y_2^0 \log a + a(x_2^1 + y_2^1 \log a + z_2^1 \log^2 a)] + O(a^2, g_0^6) \quad (18)$$

Note that the $g_0^2 \log a$ term is absent because of the renormalizability. The tree level $O(a)$ improvement leads to $y_1^1 = 0$ and $z_2^1 = 0$, while the 1-loop $O(a)$ improvement gives $x_1^1 = 0$ and $y_2^1 = 0$ in addition. In terms of the renormalized coupling at scale μ defined as

$$g_0^2 = g_R^2 - \frac{y_2^0}{x_1^0} g_R^4 \log(\mu a) = \frac{g_R^2}{1 - \frac{y_2^0}{x_1^0} \log(\mu a)} + \dots,$$

one obtains

$$\begin{aligned} X(a) &= X(0) + g_R^2 a [x_1^1 + y_1^1 \log a] \\ &\quad + g_R^4 a [x_2^1 + y_2^1 \log a + z_2^1 \log^2 a] + \dots \\ X(0) &= X_0 + g_R^2 x_1^0 + g_R^4 x_2^0 + O(g_R^6) \end{aligned}$$

The leading terms of scaling violation are $g_R^2 a$ and $g_R^4 a \log a$ for unimproved theories such as the Wilson fermion, $g_R^2 a$ and $g_R^4 a \log a$ for tree-level or tadpole $O(a)$ improved theories, or $g_R^4 a$ and $g_R^6 a \log a$ for 1-loop $O(a)$ improved theories. This concludes that a linear continuum extrapolation employed for data in the RC(TP) action[15] is justified if the $g_R^2 a$ term dominates the $g_R^4 a \log a$ term and $O(a^2)$ terms can be neglected.

Note that terms such as $(g_0^2)^n a \sim \frac{a}{(\log a)^n}$ never appear in the scaling violation, since the physical scale μ is independent on a .

5.6. Dynamical quark effect on baryon masses

Finally the dynamical quark effect on baryon masses is briefly discussed. The chiral extrapolation of baryon masses is made in terms of the PS meson mass, by the formula explicitly given as

$$\begin{aligned} m_\Sigma(s; v_1, v_2, v_2) &= A + B_s \mu_s + 2F \mu_{v_2} \\ &+ (F - D) \mu_{v_1} + C_s \mu_s^2 + (E + E_O) \mu_{v_1}^2 \\ &+ (E - E_O) \mu_{v_2}^2 + (G + G_O) \mu_s \mu_{v_1} \\ &+ (G - G_O) \mu_s \mu_{v_2} + C_{v_{12}} \mu_{v_1} \mu_{v_2} \end{aligned} \quad (19)$$

for Σ -like octet baryons, where $\mu_s = m_{\text{PS},s}^2$ and $\mu_{v_i} = m_{\text{PS}}^2(s; v_i, v_i)$. Similar formula are given for the Λ -like octet baryon mass, $m_\Lambda(s; v_1, v_2, v_2)$, and simpler ones for the decuplet baryon mass $m_D(s; v_1, v_2, v_3)$ [15].

In Fig. 12 the Σ -like octet baryon masses are plotted as a function of the averaged PS meson mass squared, $m_{\text{PS, val}}^2 = (\mu_{v_1} + 2\mu_{v_2})/3$, for the RC(TP) action[15].

To draw lines in the figure, the dynamical quark mass is kept fixed to the light quark mass, $\mu_s = m_\pi^2$. The solid line corresponds to $r_0 m_\Sigma(s; v, v, v)$ as a function of $r_0^2 \mu_v$, while the solid symbols represent N at the point of $v = s$. The error of each line, which does not include the error of r_0 , is roughly equal to the size of the symbol on the line.

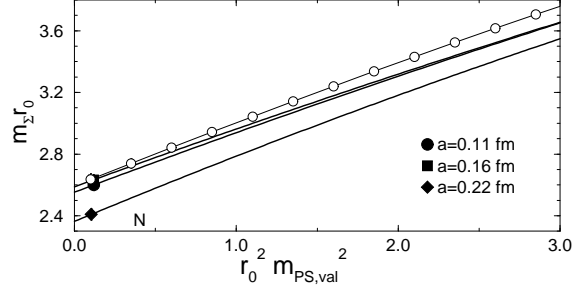


Figure 12. Σ -like octet baryon masses, normalized by r_0 , as a function of $r_0^2 m_{\text{PS, val}}^2$ for the unquenched RC(TP) action[15] and the quenched PW action[1].

The scaling violation is small at $a \leq 0.16$ fm and the slope of lines in unquenched QCD becomes flatter than that in quenched QCD, as a decreases. This may be a dynamical quark effect. One must, however, be careful to conclude this, since the physical lattice size in the simulations are different, $\simeq 2.5$ fm in unquenched simulations and 3 fm in quenched ones, so that finite size effects could make such a difference. It is therefore interesting to obtain the corresponding plot in quenched QCD with the lattice size of 2.5 fm in the continuum limit, to identify the dynamical quark effect on the slope. Moreover, even though some finite size effect is expected to exist on baryon spectra, the small scaling violation enables us to predict the chiral behavior of the baryon masses in the continuum limit with a fixed lattice size of 2.5 fm.

Similar results are obtained for the Λ -like octet baryon mass and the decuplet baryon mass. In particular almost no scaling violation is observed for the decuplet baryon mass at $a \leq 1.6$ fm.

6. Dynamical quark effect on other quantities

6.1. String breaking

In the past unquenched simulations, the expected behavior for string breaking that the static quark potential $V(R)$ levels off at large enough R , has not been observed[35–37]: $V(R)$ increases linearly in R beyond the point where it exceeds the energy of the two mesons, due to poor overlap of

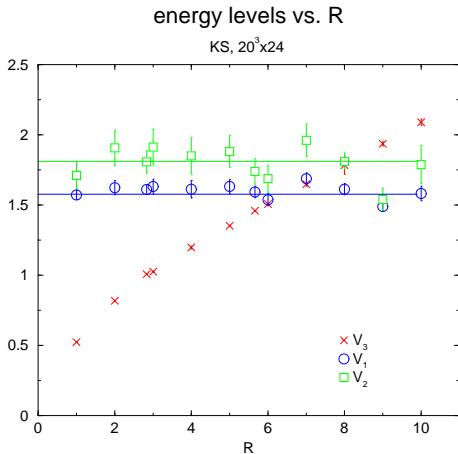


Figure 13. Lowest 3 energy levels, corresponding two S-wave mesons, S+P wave mesons and the string, as a function of the distance R .

Wilson loops with the meson-meson state.

Several variational methods have been introduced to find better operators which have larger overlap with the meson-meson state, and successfully applied to several models such as an adjoint Wilson loop in pure gauge theories or gauge-Higgs models, showing the expected behavior for “string breaking” [35].

At lattice’99 the MILC collaboration has reported a first evidence of string breaking in unquenched QCD simulations[38], and the follow-up of the result is presented at this conference[39]. They employ the $N_f = 2$ KS fermion for dynamical quarks on a $(3.3\text{fm})^3 \times (3.9\text{fm})$ lattice at $a \simeq 0.16$ fm and $m_{\text{PS}}/m_{\text{V}} = 0.36$. The energy obtained from meson-meson as well as meson-string correlators starts to level off at $R \simeq 1$ fm, where the energy is roughly equal to twice the mass of the heavy-light meson[38]. The lowest three eigen-values, obtained by the diagonalization of correlators including the string-string one, are shown in Fig. 13[39], which supports the result in ref.[38]. The mixing between the string state and the meson-meson state, however, is found to be too weak to show level crossing[39].

Let me give one comment on the definition of string breaking. String breaking should be a phenomenon that the energy for one R -independent operator linearly increases at short distance and

levels off at long distance. According to this criterion the behavior in ref. [38] is really string breaking. If one uses different operators at different R instead, the lowest energy can always be obtained by a diagonalization, even in the absence of the transition from the string state to the meson-meson state.

Apart from the string breaking, decays of hadrons, such as $\rho \rightarrow \pi\pi$, give some indications of the dynamical quark effect, since such decays are possible but largely suppressed in the quenched approximation. At this conference, the MILC collaboration presents a result which indicates the decay of $a_0(0^{++}) \rightarrow \pi(0^{-+})\eta(0^{-+})$ [33]. Contrary to the case of string breaking, the O^{++} operator employed in the simulation seems to well overlap with both a_0 and $\pi\eta$ states.

6.2. Topological susceptibility

From the flavor-singlet axial Ward-Takahashi(WT) identity in the continuum,

$$\begin{aligned} & \langle (\partial^\mu A_\mu(x) + 2m_q P(x))Q(y) \rangle \\ & + 2N_f \langle Q(x)Q(y) \rangle = 0, \end{aligned} \quad (20)$$

one obtains

$$-2m_q \int d^4x \langle P(x)Q \rangle = 2N_f \langle Q^2 \rangle, \quad (21)$$

where $Q = \int d^4x Q(x)$ is the topological charge with the topological charge density $Q(x) = \frac{g^2}{32\pi^2} \frac{1}{2} F_{\mu\nu}(x) \tilde{F}^{\mu\nu}(x)$. Therefore

$$\chi \equiv \frac{\langle Q^2 \rangle}{V} = -\frac{m_q}{N_f V} \int d^4x \langle P(x)Q \rangle \rightarrow 0 \quad (22)$$

as $m_q \rightarrow 0$. The topological susceptibility χ must vanish in the chiral limit. An investigation of this property on the lattice becomes a good check for lattice chiral symmetry in unquenched simulations. The decrease of χ toward $m_q = 0$ is driven purely by the fermion determinant.

In the past simulations, the expected decrease of χ has not been observed for both KS[41] and Wilson-type[15] quark actions. The topological susceptibility normalized by R_0 does not show the quark mass dependence at all and values are consistent with the quenched one[15].

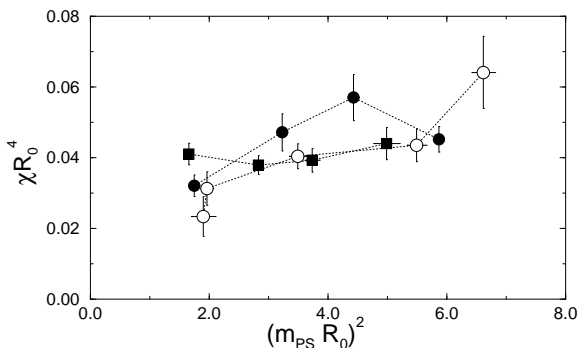


Figure 14. χR_0^4 as a function of $m_{\text{PS},s}^2 R_0^2$ in $N_f = 2$ unquenched QCD for the PC(NP) action (open circles) [42] at $a \simeq 0.1$ fm and for the RC(TP) action (solid symbols) at $a \simeq 0.11$ fm (circles) [43] and 0.16 fm (squares) [15].

This year the UKQCD collaboration [42] and CP-PACS collaboration [43] have obtained new results, which are shown in Fig. 14. The decrease of χ toward the chiral limit is observed at $a \simeq 0.1$ fm for both PC(NP) and RC(TP) actions, in contrast to the previous result at $a = 0.16$ fm for the RC(TP) action, though it is still far from verifying the flavor-singlet axial WT identity. Theoretical considerations [44] as well as further numerical analyses are needed to settle this issue completely.

6.3. Flavor-singlet PS meson

The fact that the flavor-singlet pseudo-scalar meson is not a Nambu-Goldstone boson (U(1) problem) must be demonstrated by lattice QCD simulations. Numerically this has been a difficult task since one has to calculate the quark 2-loop diagram special for the flavor-singlet meson. By the volume-sources method without gauge-fixing [45] or the U(1) random noise method [46] the estimation of the flavor-singlet meson mass becomes possible in quenched QCD.

The calculation of the singlet meson mass appears to be much harder in unquenched QCD, where the individual meson propagators should behave as

$$\langle \eta(0)\eta(t) \rangle_{2\text{-loop}} \simeq Z_\pi e^{-m_\pi t} - Z_\eta e^{-m_\eta t} \quad (23)$$

$$\langle \eta(0)\eta(t) \rangle_{1\text{-loop}} \simeq Z_\pi e^{-m_\pi t}. \quad (24)$$

Here $\eta = \bar{q}\gamma_5 \mathbf{1}q$ is the flavor-singlet PS meson

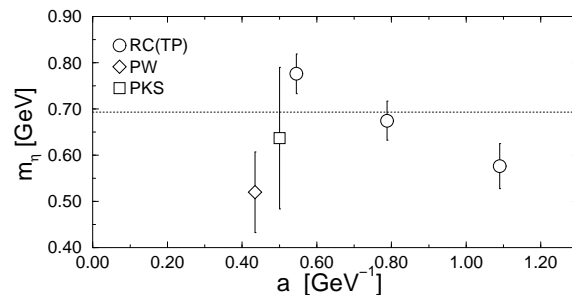


Figure 15. m_η in GeV as a function of a in $N_f = 2$ unquenched QCD for RC(TP) [15], PW [47] and PKS [46]. The smearing source is employed for the latter two. The horizontal line is the “experimental” value of the flavor-singlet meson mass in $N_f = 2$ QCD.

operator, m_η is the corresponding mass and m_π is the mass of the degenerate non-singlet PS meson. Since the pole of the η appears after the leading contribution of π is completely canceled between two diagrams, the signal becomes too noisy at large t to extract m_η .

Therefore one is forced to extract m_η at small t , and one usually fits the ratio of propagators as [46]

$$R(t) = \frac{\langle \eta(0)\eta(t) \rangle_{2\text{-loop}}}{\langle \eta(0)\eta(t) \rangle_{1\text{-loop}}} \simeq 1 - \frac{Z_\eta}{Z_\pi} e^{-(m_\eta - m_\pi)t},$$

hoping that a large part of contributions from excited states may be canceled out in the ratio. The CP-PACS collaboration [15] indeed found that $m_\eta - m_\pi$ extracted from the ratio for $t_{\min} = 2$ is consistent with the one for $t_{\min} = 3, 4$ within statistical errors, where t_{\min} is the minimum value of t for the fit.

Recently the SESAM-T χ L collaboration has shown [47] that the plateau for m_η as well as m_π starts at reasonably small t , employing the smearing source. This opens a possibility for a reliable calculation of m_η in very near future.

In the chiral limit one obtains a non-zero value of m_η [46, 15, 47], which is shown in Fig. 15 as a function of a , together with the value of $m_\eta \simeq 0.7$ GeV for $N_f = 2$ QCD derived from the experimental value ($N_f = 3$) by the Witten-Veneziano formula [48]. Although results from different actions seems consistent within large errors, the re-

sult from the RC(TP) action show a systematic increase toward the continuum limit. One has to check if this large scaling violation is caused by the contamination from excited states to the ground state in the ratio $R(t)$.

A new calculation with the smearing source on configurations of the CP-PACS collaboration will make it possible to extract m_η reliably in the continuum limit of $N_f = 2$ QCD, while the inclusion of the mixing to $\bar{s}s$ state[49] as well as the dynamical strange quark will be necessary for the final result in $N_f = 3$ QCD.

7. Summary

We surprisingly find that hadron spectra from quenched QCD disagree in the continuum limit between KS and Wilson quark actions. This discrepancy has to be resolved as soon as possible. Personally I feel that some problems may exist in the identification of particles in KS quark actions, in particular of baryons. The restoration of the flavor breaking in hadron spectra might be a good check. Hadron spectra from domain-wall and overlap quark actions[50] may also give an important hint for the solution.

Within Wilson-type quark actions, the $N_f = 2$ dynamical quark effect on hadron spectra, in particular in meson masses, has been demonstrated. Both chiral and continuum extrapolations are important to identify the effect. Results for baryons suggest that the scaling violation is small but the lattice size has to be increased for reliable predictions in the continuum limit. Decreasing the dynamical quark mass will also be the next challenge in unquenched simulations.

The dynamical quark effect becomes manifest in some other quantities such as the string breaking, the topological susceptibility and the flavor-singlet meson mass, even at finite lattice spacing.

New direction of investigations in unquenched QCD will be opened by realistic $N_f = 2 + 1$ unquenched simulation, which is the last step to numerically solve QCD. Promising algorithm for $N_f = 2 + 1$ QCD seems HMC for $N_f = 2$ light quarks and PHMC[51] for the $N_f = 1$ strange quark. Some results will be expected at the first lattice conference in the next century.

Acknowledgements

I would like to thank C. Allton, J.M. Carmona, A. Hart, A. Irving, K. Ishikawa, D.B. Leinweber, J.W. Negele, H. Panagopoulos, R. Parthasarathy, G. Rossi, S. Sharpe, D. Toussaint, U. Wolff and T. Yoshie for communicating and providing their results, and, in particular, R. Burkhalter, C. DeTar, S. Gottlieb and T. Kaneko in addition for making new data I have requested. I also thank R. Burkhalter, Y. Iwasaki, T. Kaneko, S. Hashimoto and A. Ukawa for valuable comments on the manuscript. This work is supported in part by the Grants-in-Aid of Ministry of Education(Nos. 12014202, 12640253).

REFERENCES

1. S. Aoki *et. al.* (CP-PACS collaboration), Phys. Rev. Lett 84 (2000) 238.
2. V. Lubicz, "Quark mass on lattice: Light and heavy", these proceedings.
3. L. Lellouch, "Light hadron weak matrix elements", these proceedings.
4. C. Bernard, "Properties of heavy-light and heavy-heavy hadrons, and constraints on the unitarity triangle", these proceedings.
5. Y. Iwasaki, Nucl. Phys. B258 (1985) 141; Univ. of Tsukuba report UTHEP-118(1983), unpublished.
6. M. Lüscher and P. Weisz, Commun. Math. Phys. 97 (1985) 59; P. Weisz, Nucl. Phys. B212 (1983) 1.
7. S. Naik, Nucl. Phys. B316 (1989) 238.
8. K. Orginos, D. Toussaint and R.L. Sugar, Phys. Rev. D60 (1999) 054503; Nucl. Phys. B(Proc. Suppl.) 83-84 (2000) 878.
9. B. Sheikholeslami and R. Wohlert, Nucl. Phys. B259 (1985) 572.
10. N. Eicker *et. al.* (SESAM collaboration), Phys. Rev. D59 (1999) 014509.
11. T. Lippert *et. al.* (SESAM-T χ L collaboration), Nucl. Phys. B(Proc.Suppl.) 60A (1998) 311.
12. R. Mawhinney, Nucl. Phys. B(Proc.Suppl.) 83-84 (2000) 57 and references therein.
13. C. Bernard *et. al.* (MILC collaboration), Nucl. Phys. B(Proc.Suppl.) 73 (1999) 198;

- 60A (1998) 297 and references therein.
14. C.R. Allton *et al.* (UKQCD Collaboration), Phys. Rev. D60 (1999) 034507.
 15. R. Burkhalter, Nucl. Phys. B(Proc.Suppl.) 73 (1999) 3; S. Aoki *et al.* (CP-PACS collaboration), *ibid.* 73 (1999) 192; A. Ali Khan *et al.* (CP-PACS collaboration), *ibid.* 83-84 (2000) 176; hep-lat/0004010; these proceedings.
 16. A.C. Irving (UKQCD Collaboration), these proceedings.
 17. S. Aoki *et al.* (JLQCD Collaboration), these proceedings.
 18. C. Bernard *et al.* (MILC Collaboration), Phys. Rev. D62 (2000) 034503.
 19. Th. Lippert, S. Güsken and K. Schilling, Nucl. Phys. B(Proc.Suppl.) 83-84 (2000) 182.
 20. Y. Kuramashi *et al.*, Phys. Lett. B313 (1993) 425; B. Allés *et al.*, *ibid.* B389 (1996) 107.
 21. The long auto-correlation time of Q with the KS action may be reduced by the parallel tempering method. See E.-M. Ilgenfritz *et al.*, hep-lat/0007039.
 22. M. Fukugita *et al.*, Phys. Rev. Lett. 68 (1992) 761; Phys. Lett. B294 (1992) 380; Phys. Rev. D47 (1993) 4739; S. Aoki *et al.*, *ibid.* D50 (1994) 486.
 23. C. Bernard *et al.* (MILC Collaboration), Phys. Rev. D48 (1993) 4419.
 24. R. Sommer, Nucl. Phys. B411 (1994) 839.
 25. S. Tamhankar and S. Gottlieb, Nucl. Phys. B(Proc.Suppl) 83-84 (2000) 212.
 26. B. Bolder *et al.* (SESAM-T χ L Collaboration), hep-lat/0003012.
 27. M. Lüscher *et al.* (ALPHA collaboration), Nucl. Phys. B478 (1996) 365.
 28. S. Sint and R. Sommer, Nucl. Phys. B465 (1996) 71.
 29. G. Martinelli *et al.*, Phys. Lett. B411 (1997) 141.
 30. C. Bernard *et al.* (MILC Collaboration), Phys. Rev. Lett. 81 (1998) 3087.
 31. S. Sharpe, Nucl. Phys. B(Proc.Suppl.) 34 (1994) 403.
 32. C. Bernard *et al.* (MILC Collaboration), Phys. Rev. D61 (2000) 111502.
 33. C. Bernard *et al.* (MILC Collaboration), these proceedings.
 34. K.C. Bowler *et al.* (UKQCD Collaboration), Nucl. Phys. B(Proc.Suppl) 63 (1998) 182; Phys. Rev. D62 (2000) 054506.
 35. K. Schilling, Nucl. Phys. B(Proc.Suppl) 83-84 (2000) 140 and references therein.
 36. S. Aoki *et al.* (CP-PACS collaboration), Nucl. Phys. B(Proc.Suppl.) 73 (1999) 216.
 37. B. Bolder *et al.* (SESAM-T χ L Collaboration), hep-lat/0005018.
 38. C. Detar, U. Heller and P. Lacock, Nucl. Phys. B(Proc.Suppl) 83-84 (2000) 310.
 39. C. Bernard *et al.* (MILC Collaboration), these proceedings.
 40. P. Pennanen and C. Michael (UKQCD collaboration), hep-lat/0001015 .
 41. B. Allés *et al.*, hep-lat/9909045; hep-lat/0004020.
 42. A. Hart and M. Teper (UKQCD collaboration), hep-lat/0004180.
 43. S. Aoki *et al.* (CP-PACS collaboration), in preparation.
 44. Some subtleties exist in the flavor-singlet lattice WT-identity: G. Rossi and M. Testa, private communication.
 45. Y. Kuramashi *et al.*, Phys. Rev. Lett. 72 (1994) 3448.
 46. G. Kilcup *et al.*, Nucl. Phys. B(Proc.Suppl) 47 (1996) 358; L. Venkatamaran *et al.*, *ibid.* 53 (1997) 259.
 47. T. Struckmann *et al.* (SESAM-T χ L Collaboration), hep-lat/0006012; hep-lat/0010005.
 48. E. Witten, Nucl. Phys. B156 (1979) 269; G. Veneziano, *ibid.* B159 (1979) 213.
 49. C. Michael *et al.* (UKQCD collaboration), Nucl. Phys. B(Proc.Suppl.) 83-64 (2000) 162. C. McNeile and C. Michael (UKQCD collaboration), hep-lat/0006020.
 50. P. Vranas, "Domain-wall fermions and applications", these proceedings.
 51. T. Takaishi and P. de Forcrand, Nucl. Phys. B(Proc.Suppl.) 53 (1997) 968; these proceedings; R. Frezzoti and K. Jansen, Phys. Lett. B402 (1997) 328.